



# Change in strong Eastern Pacific El Niño events dynamics in the warming climate

Aude Carréric<sup>1,2</sup> · Boris Dewitte<sup>1,3,4,5</sup> · Wenju Cai<sup>6,7</sup> · Antonietta Capotondi<sup>8,9</sup> · Ken Takahashi<sup>10</sup> · Sang-Wook Yeh<sup>11</sup> · Guojian Wang<sup>6,7</sup> · Virginie Guémas<sup>12</sup>

Received: 15 March 2019 / Accepted: 28 October 2019 / Published online: 9 November 2019  
© Springer-Verlag GmbH Germany, part of Springer Nature 2019

## Abstract

While there is evidence that ENSO activity will increase in association with the increased vertical stratification due to global warming, the underlying mechanisms remain unclear. Here we investigate this issue using the simulations of the NCAR Community Earth System Model Large Ensemble (CESM-LE) Project focusing on strong El Niño events of the Eastern Pacific (EP) that can be associated to flooding in Northern and Central Peru. It is shown that, in the warmer climate, the duration of strong EP El Niño events peaking in boreal winter is extended by two months, which results in significantly more events peaking in February–March–April (FMA), the season when the climatological Inter-Tropical Convergence Zone is at its southernmost location. This larger persistence of strong EP events is interpreted as resulting from both a stronger recharge process and a more effective thermocline feedback in the eastern equatorial Pacific due to increased mean vertical stratification. A heat budget analysis reveals in particular that the reduction in seasonal upwelling rate is compensated by the increase in anomalous vertical temperature gradient within the surface layer, yielding an overall increase in the effectiveness of the thermocline feedback. In CESM-LE, the appearance of strong EP El Niño events peaking in FMA accounts for one-quarter of the increase in frequency of occurrence of ENSO-induced extreme precipitation events, while one-third results from weak-to-moderate El Niño events that triggers extreme precipitation events because of the warmer mean SST becoming closer to the convective threshold. In CESM-LE, both the increase in mean EP SST and the change in ENSO processes thus contribute to the increase in extreme precipitation events in the warmer climate.

**Keywords** CESM-LE · Extreme El Niño event · Climate change · Vertical stratification

## 1 Introduction

El Niño–Southern Oscillation (ENSO) is the most important mode of inter-annual variability in the tropical Pacific. By impacting meteorological conditions worldwide via atmospheric teleconnections (Ropelewski and Halpert 1987; Yeh et al. 2018), it leads to dramatic societal and economics impacts (McPhaden et al. 2006). Understanding if and how El Niño characteristics will change with global

warming has been a major concern since the first Coupled Model Intercomparison Projects in the 1990s (Meehl et al. 2000). While large progresses in our vision of the likely changes in ENSO statistics have been made in the recent decades (Yeh et al. 2009a; Power et al. 2013; Cai et al. 2014, 2015b), there are still many uncertainties in the mechanisms at play to explain the changes in statistics in the context of global warming, all the more so as models have persistent biases [e.g. westward shift in the center of action of El Niño (Zheng et al. 2012; Li and Xie 2013), double Inter-Tropical Convergence Zone (ITCZ) syndrome (Hwang and Frierson 2013; Li and Xie 2013), warm bias in the far eastern Pacific (Richter 2015)]. These biases can in particular impact the realism of ENSO diversity in models (Ham and Kug 2012; Karamperidou et al. 2017) by, for instance, influencing the evolution of sea surface temperature (SST) anomalies during El Niño development (Santoso et al. 2013; Dewitte and Takahashi 2017), favoring so-called double peaked El Niño

**Electronic supplementary material** The online version of this article (<https://doi.org/10.1007/s00382-019-05036-0>) contains supplementary material, which is available to authorized users.

✉ Aude Carréric  
aude.carrerice@gmail.com

✉ Boris Dewitte  
boris.dewitte@ceaza.cl

Extended author information available on the last page of the article

events (Graham et al. 2017) or yielding compensating errors amongst the main ENSO feedbacks (Bayr et al. 2018). Since ENSO diversity is also a manifestation of the non-linearity of ENSO (Takahashi et al. 2011; Capotondi et al. 2015) that can impact mean state changes at low-frequency (Lee and McPhaden 2010; McPhaden et al. 2011; Choi et al. 2012; Karamperidou et al. 2017), these biases are also likely influential on the way models simulate internal variability (Zheng et al. 2018). This has been a limitation to gain confidence in the projections of ENSO changes by these same models, but also to infer a clear mechanistic understanding of the sensitivity of ENSO to climate change.

So far, two broad views of the mechanisms at work in ENSO change due to global warming have been documented: (1) the projected faster warming of the eastern equatorial Pacific compared to that of the central Pacific will induce an easier eastward shift of the convection area from the central Pacific, through a weakening of westward mean equatorial currents associated with the reduction of the equatorial trade winds (Vecchi and Harrison 2006; Santoso et al. 2013); (2) the faster eastern equatorial Pacific surface warming due to climate change will reduce the meridional SST gradient in the eastern Pacific so that the ITCZ is likely to move more often southward, inducing an increase in the number of ENSO-induced extreme precipitation events in the eastern Pacific (Power et al. 2013; Cai et al. 2014, 2015b, 2017). Note that this applies to the warm phase of ENSO and not to the cold phase (La Niña) for which the faster warming of the Maritime continent in the Indonesian sector will tend to facilitate extreme La Niña events (Cai et al. 2015a).

Although these paradigms of the impact of climate change on ENSO provide useful guidance for analyzing and interpreting models, they present two main related caveats: first, they allow explaining the increase in ENSO-related extreme precipitation events but do not address changes in ENSO statistics itself. In particular, the increase in extreme precipitation events does not necessarily require that El Niño events become stronger. This issue is nevertheless relevant considering the oceanographic consequences of strong El Niño events on the marine ecosystems in particular along the coast of Peru and Chile (Barber and Chavez 1983; Carr et al. 2002). Second, in their principles, these paradigms only consider changes in surface processes (mixed-layer) although the latter are tightly linked to dynamical changes associated with thermocline processes. In particular, the differential warming between the surface oceanic layer and the thermocline under anthropogenic forcing yields a significant increase in vertical stratification across the equatorial Pacific (Yeh et al. 2009a; DiNezio et al. 2009; Capotondi et al. 2012) that can be influential on ENSO dynamics through a number of processes. Not only it modulates the way the wind stress forcing projects on the wave dynamics (Dewitte et al. 1999, 2009), influencing ENSO stability (Dewitte et al.

2007; Thual et al. 2013), but it also directly influences the so-called thermocline feedback, that is the sensitivity of SST to thermocline fluctuations (Zelle et al. 2004), a key process during Eastern Pacific (EP) El Niño events (Zebiak and Cane 1987; An and Jin 2001). The effect of changes in vertical stratification on ENSO dynamics in the context of global warming has been suggested in former studies (Yeh et al. 2009a, b, 2010; DiNezio et al. 2009; Stevenson et al. 2017). Recently it has been shown that the variance of EP El Niño events increases in association with the stronger vertical stratification in the central Pacific in a set of models that realistically simulate the non-linear character of ENSO (Cai et al. 2018). While this study consolidates the confidence in climate change projections by showing a large inter-model consensus with regards to their sensitivity to changes in vertical stratification, the statistical approach somehow limits a clear understanding of the oceanic processes involved. It thus calls for advancing our mechanistic understanding of the sensitivity of EP El Niño events to changes in vertical stratification in the context of climate change. In particular, the main question that motivates the present work is: Through which processes are strong EP El Niño events favored in the warmer climate and how does their increase in frequency explain the increased occurrence of extreme precipitation events?

Here we take advantage of the simulations of the CESM-LE project (Kay et al. 2015) to investigate the mechanisms behind the sensitivity of ENSO statistics to mean state changes focusing on strong EP El Niño events that are those associated with extreme events (Takahashi et al. 2011; Takahashi and Dewitte 2016, hereafter TD16). The CESM-LE project provides a large number of realizations of the same model, the NCAR Community Earth System Model (CESM), a Coupled General Circulation Model (CGCM) that accounts for ENSO diversity with some skill (Stevenson et al. 2017; Dewitte and Takahashi 2017). The CESM model also simulates changes in mean SST pattern between the present climate (historical) and the climate corresponding to RCP8.5 future greenhouse gas emission scenarios (hereafter RCP8.5) comparable to those of the CMIP5 ensemble mean (Vecchi and Soden 2007; Li et al. 2016), that is an El Niño-like pattern warming. Finally, this model also predicts an increase in ENSO-related extreme precipitation events in a warmer climate comparable to that of the CMIP5 ensemble (Cai et al. 2014), thus offering a perfect test-bed for better understanding the relative influence of the gradual SST warming and the changes in ENSO dynamics on the statistics of extreme precipitation events.

The paper is organized as follows: after describing the data sets and the methods used in Sect. 2, we document the changes in ENSO statistics due to global warming (Sect. 3), highlighting changes in the seasonality of the number of events. Section 4 presents a heat budget analysis where

changes in the composite evolution of the tendency terms associated with global warming are interpreted in the light of an analysis of change in the thermocline feedback in the model. Section 5 is a discussion followed by concluding remarks.

## 2 Data and method

### 2.1 Data

We use long-term simulations of the NCAR Community Earth System Model Large Ensemble Project (CESM-LE) (Kay et al. 2015). The 42 and 40 members of the historical runs (1850–2005 for one member, 1920–2005 otherwise) and RCP8.5 runs (2006–2100) are respectively used here consisting in a total of 3682 and 3800 years, which allows estimating the spread between members and thus confidence levels in the statistics (estimated by a Wilcoxon rank sum test in this study).

As defined by the CMIP5 design protocol (Taylor et al. 2012), the historical external forcing is composed of the observed atmospheric composition changes due to emissions of greenhouse gases and aerosols and the natural volcanic and orbital forcing. The RCP8.5 scenario corresponds to a “representative concentration pathways” (RCP) of high emissions of greenhouse gases, where the 8.5 label corresponds to an estimation of the radiative forcing ( $8.5 \text{ W/m}^2$ ) at the end of the simulation that is the year 2100.

The simulations of the CESM-LE project use the Community Earth System Model, version 1 (CESM1) (Hurrell et al. 2013) coupling the Community Atmosphere Model version 5 (CAM5) atmosphere component (Meehl et al. 2013), the Los Alamos National Laboratory (LANL) Parallel Ocean Program version 2 (POP) ocean component (Smith et al. 2010), the Community Land model version 4 (CLM4) land component (Oleson et al. 2010) and the LANL Community Ice CodE (CICE4) sea ice component (Hunke and Lipscomb 2010). All components of the model are approximately  $1^\circ$  horizontal resolution. The atmospheric component has 30 vertical levels, the oceanic component has 60 vertical layers. CESM1(CAM5) still presents some of the persistent biases of coupled models, such as a westward shift of the cold tongue, the double ITCZ and an excessive mean precipitation in the tropical Pacific (Hurrell et al. 2013). However, as its previous version CCSM4, CESM1(CAM5) correctly simulates some intrinsic characteristics of ENSO such as a realistic 3–6 years period but overestimates the magnitude compared to observations (Gent et al. 2011; Deser et al. 2012; Hurrell et al. 2013). The seasonality of the ENSO variance is well represented despite the magnitude bias and a larger difference between winter and summer. It implies that the observed variance values are outside the simulated

CESM-LE internal variability for certain months of the year (January to April) (Zheng et al. 2018). This model also accounts for many ENSO properties, in particular its diversity (Stevenson et al. 2017; Dewitte and Takahashi 2017). Karamperidou et al. (2017) and Cai et al. (2018) showed the importance of ENSO non-linearities in the response of the tropical Pacific to global warming. The metric of non-linearity  $\alpha$  defined by Karamperidou et al. (2017) and consisting in the leading coefficient of the parabolic approximation of the ENSO variability in the first and second principal components (PC) of SST anomalies in the tropical Pacific space, is used here as an integrated measure of diversity (see also Dommenget et al. (2013) for such an approach). It yields a value  $\alpha = -0.37 \pm 0.08$  ( $\pm 22\%$ ) for the CESM-LE historical run, which is close to the estimate from HadISST v1.1 observations (1950–2017) ( $\alpha = -0.39$ ) and from some CMIP5 models (Karamperidou et al. 2017; Cai et al. 2018). In particular, the  $\alpha$  value for the CESM ensemble is lower than the threshold value for  $\alpha$  used in Cai et al. (2018) (i.e.  $\alpha = -0.15$ ) to discriminate non-linear models. The CESM model has thus a non-linear behavior similar to that of the ensemble model used in Cai et al. (2018).

Stevenson et al. (2017) showed that the ENSO diversity in the CESM model is sensitive to various forms of external forcing using the Last Millennium Ensemble that contains many realizations of the 850–2005 period with differing combinations of forcing. In particular, anthropogenic changes in greenhouse gases and ozone/aerosol emissions can alter the persistence of EP and CP El Niño events, although forced changes in ENSO amplitude are generally small because of compensating effects between changes in oceanic processes. Here since we focus on the RCP8.5 scenario that corresponds to a significantly larger external forcing on the mean climate, we expect to identify more pronounced changes in ENSO processes, aided by our methodological approach to derive robust ENSO diversity changes in models (See Sect. 2.2).

The HadISST v1.1 monthly average sea surface temperature dataset (Rayner 2003) is used to estimate whether the representation of the internal climate variability spread simulated by the members of CESM-LE includes the observed contemporary climate trajectory. The dataset has a resolution grid of  $1^\circ$  latitude-longitude. We use the period from January 1950 to December 2017.

### 2.2 Definition of El Niño events and extreme precipitation events

#### 2.2.1 El Niño events

Considering that at least two indices should be used in order to account for the different locations of SST anomalies peaks (Trenberth and Stepaniak 2001; Takahashi et al.

2011; Ren and Jin 2011; Dommenget et al. 2013), we use the E and C indices defined by Takahashi et al. (2011) as  $E = (PC1 - PC2)/\sqrt{2}$  and  $C = (PC1 + PC2)/\sqrt{2}$  where the PC1 and PC2 are the normalized principal components of the first two empirical orthogonal function (EOF) modes of SST anomalies in the tropical Pacific (120° E–290° E; 10° S–10° N). The E and C indices are thus linearly uncorrelated by construction. They are calculated separately for the two different periods (historical versus RCP8.5). The SSTs are linearly detrended and the seasonal cycle is removed for each period and for each member independently, prior to carrying the EOF decomposition. A bilinear regression of the SST anomalies onto these indices is used to determine the SST anomalies spatial patterns associated with each index (Fig. 1), indicating a relative good agreement between model and observations, although CESM simulates the center of the patterns displaced to the west compared to observations by 20° and 30° for the E and C patterns respectively. This westward bias of the SST variability is comparable to the CMIP5 ensemble (cf. Fig. 1 of Matveeva et al. (2018)). Note also the cold tongue bias as evidenced by the position of the mean 28 °C isotherm in Fig. 1, that is shifted westward by 25°, a feature common to many other CGCMs (Wittenberg et al. 2006; Bellenger et al. 2014). These biases have been detrimental for comparing observations and models, particularly from historical ENSO indices, because the use of fixed regions (e.g. Niño-3) for averaging quantities results in differences that reflect this shift in variability and mean state rather than the actual dynamics of the system. For instance, Graham et al. (2017) showed that the recurrent CGCMs equatorial Cold Tongue bias can lead to the simulation of “fake” El Niño events that have never been observed, double peaking in the tropical band and called “double peaked” El Niño events. Using the conventional Niño regions to define

El Niño diversity increases the risk of integrating so-called “double peaked” El Niño events and mistaking them as CP El Niños when compositing, although they have more commonalities with the observed EP El Niño events. We thus follow the methodology of TD16 which projects tropical Pacific variability (and feedbacks) onto the E and C modes rather than fixed regions to avoid these limitations (see Sect. 2.3.). Note that this method has proven to be skillful in showing a strong inter-model consensus on the SST variability of EP El Niño events despite differences in the details of El Niño simulation across models (Cai et al. 2018).

In order to diagnose changes in ENSO statistics between the present and future climates, we estimate the E and C modes for the two periods, the historical period (1920–2005) and the RCP8.5 period (2006–2100), which provides two sets of E and C modes (patterns and time-series). The change in statistics is therefore reflected here in both the pattern and the temporal evolution of the modes. This is motivated by the fact that the ENSO pattern is changing between the present and future climate (Fig. 2). The E and C indices have been normalized so that the patterns can be expressed in °C. In particular, there is a westward amplification (by 20°) of the E mode and an eastward amplification (by 35°) of the C mode in the warmer climate. In order to take into account these changes in the spatial patterns, the E and C indices of the RCP8.5 simulations are scaled by the projection of the associated spatial pattern on its counterpart of the historical runs. The scaling coefficients are equal to  $1.16 \pm 10\%$  ( $\pm 0.12$ ) for both E and C modes over 10° S–10° N. This allows comparing changes in the amplitude of the composite evolution of the E and C indices (Fig. 3) and not just changes in temporal evolution. Note that this method yields similar results than the one used in Cai et al. (2018),

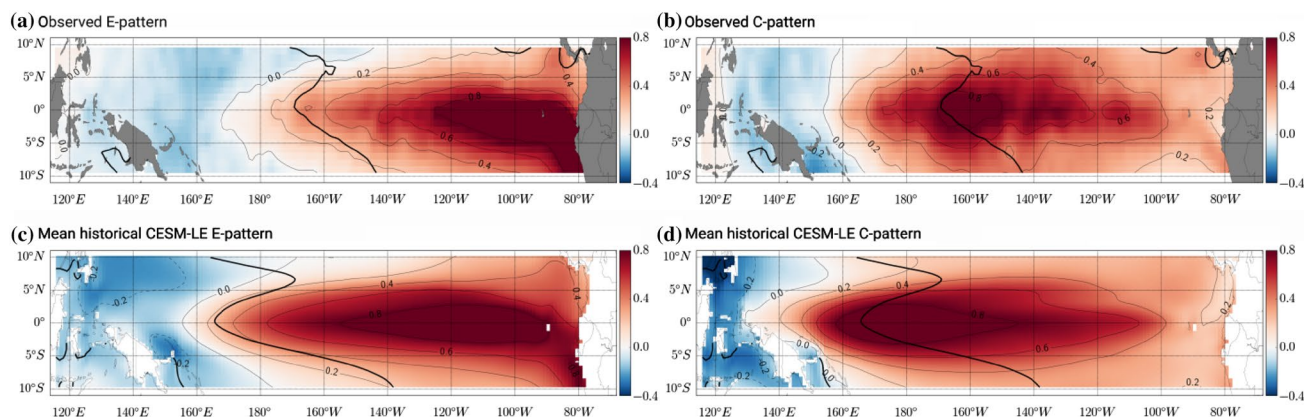


**Fig. 1** Linear regression coefficients (°C) of SST anomalies onto the E (a, c) and C (b, d) indices for (a, b) HadISST v1.1 (1950–2017) and (c, d) the ensemble mean of CESM-LE historical simulations (42 members). The E and C indices are defined from the two leading

principal components of the EOF analysis of the SST anomalies in the tropical Pacific (115° E–290° E; 10° S–10° N). The SST anomalies are linearly detrended over each time period. Also shown is the mean position of the 28 °C isotherm (thick black line)

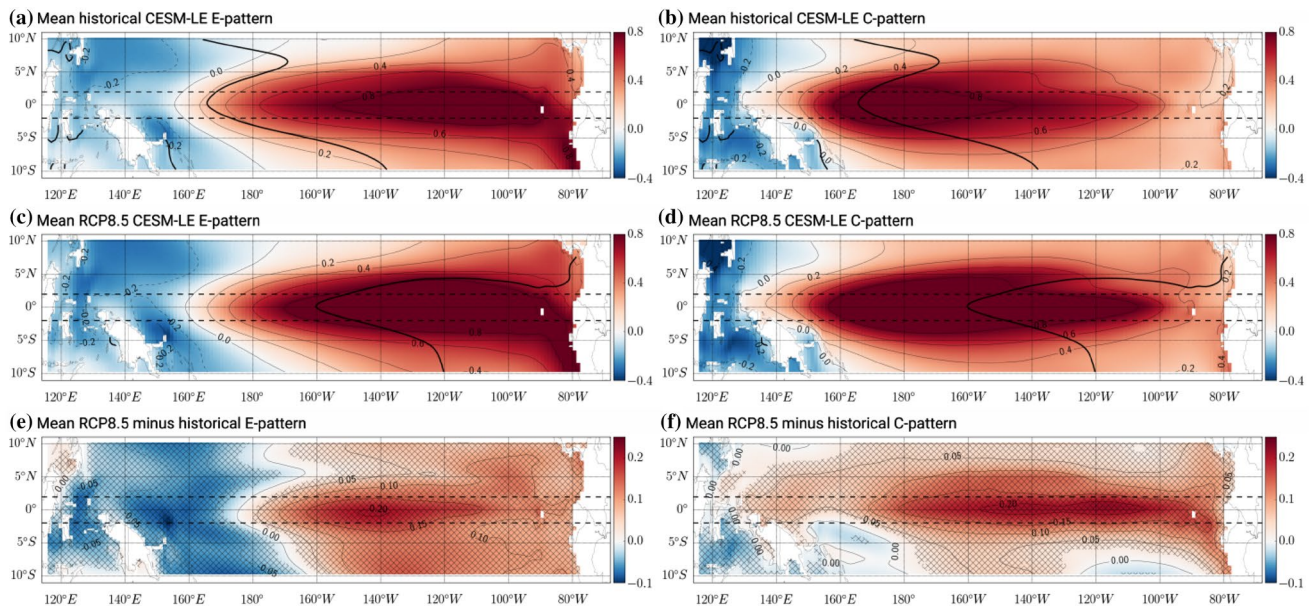


**Fig. 2** Ensemble mean of the linear regression coefficients ( $^{\circ}\text{C}$ ) of SST anomalies onto the E (left) and C (right) indices calculated for the historical runs (a, b), the RCP8.5 runs (c, d) and the differences between RCP8.5 and historical runs (e, f). The E and C indices are defined from the two leading principal components of the EOF analysis of the SST anomalies in the tropical Pacific ( $115^{\circ}\text{E}$ – $290^{\circ}\text{E}$ ;  $10^{\circ}\text{S}$ – $10^{\circ}\text{N}$ ). The SST anomalies are linearly detrended over each

time period. The 5% confidence intervals from a Wilcoxon rank-sum test are indicated by stippling. The stippling indicates where the values of the RCP8.5 runs are significantly larger (in absolute value) than that of the historical runs. Note the different scale of the colorbar on e and f. In the dashed lines is indicated the  $2^{\circ}\text{S}$ – $2^{\circ}\text{N}$  region onto which the heat budget is projected

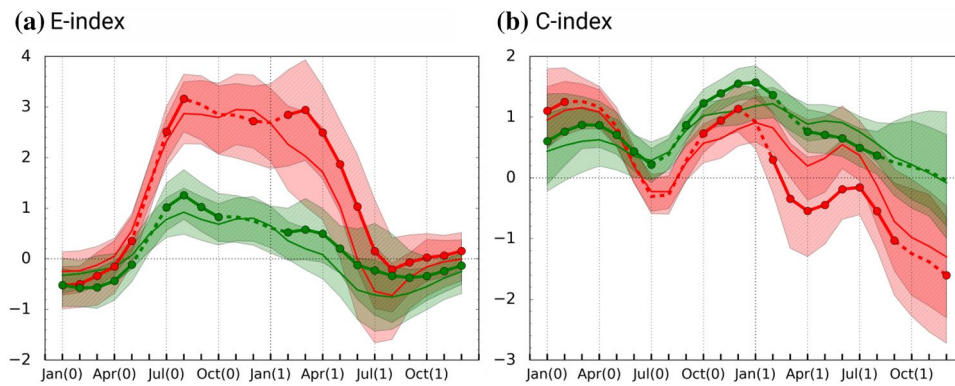


**Fig. 3** Composite evolution of a the E and b the C indices ( $115^{\circ}\text{E}$ – $290^{\circ}\text{E}$ ;  $10^{\circ}\text{S}$ – $10^{\circ}\text{N}$ ) during strong (red) and moderate (green) El Niño events for (solid lines) historical and (lines with circles) RCP8.5 runs. The shading indicates the range of values between

the 25th and 75th percentiles of the distribution. The portion of the curves in dashed line for the RCP8.5 composites indicates where the changes between historical and RCP8.5 are not significant at the 95% level according to a Wilcoxon rank sum test

that does not consider change in spatial patterns of the E and C modes, but instead performs an EOF analysis of SST anomalies over the whole record (1920–2100). In particular, the increase in the variance of the E index in DJF from historical to RCP8.5 runs is 14% for our method and 18% for the Cai et al. (2018)’s method when considering the last 85 years of each period. The largest difference in methods is the dispersion amongst the members that is

in general larger in the method used here. Despite these differences, we find that the increase in variance of the E index in DJF is significant at the 95% confidence level based on a Wilcoxon test for both methods. CESM simulates thus an increase in the DJF E-index variance in the future climate, regardless of the method, comparable to 17 models of the CMIP5 data base that account realistically for the non-linear behavior of ENSO (Cai et al. 2018).

El Niño events are defined from the PC1 derived from the analysis of the main mode of variability of the tropical Pacific by the EOF method. El Niño events are when the value of the PC1 exceeds its 75% percentile over at least 5 consecutive months, regardless of season. Our definition is slightly different from that of TD16 that seek for El Niño peaks over 2-year running mean time windows with a 1–2–1 filter applied to the PC1. We checked that both methods provide very comparable statistics by applying our definition to the GFDL CM2.1 PI-control simulation and comparing our results with that of TD16. In the meantime, it has been also verified that using the historical definition by the ONI index does not change ENSO statistics on the PI-control simulation of CESM. El Niño classes (strong versus moderate) are then defined based on the E index. When the E-index value reaches a threshold value (interpreted here as the value of SST anomalies in the far eastern Pacific needed for deep convection to be activated), a strong EP event takes place. This threshold is estimated from a *k-mean* cluster analysis ( $k=2$ ) applied jointly to the E and C values during El Niño years and for the calendar month when the E-index is maximal. It yields two classes that correspond to moderate (either EP or CP) Niño events (cluster 1) and strong EP El Niño events (cluster 2). We find a threshold value of 2.2 °C for the PI-control simulation (see also Dewitte and Takahashi (2017)). Note that the PI-control and historical simulations of CESM do not exhibit a well-defined bimodal distribution in the (E, C) space conversely to the GFDL CM2.1 model (see TD16), so that the determination of this threshold value is somewhat subjective and certainly sensitive to the model biases. Nevertheless the model exhibits a clear non-linearity in the response of the wind stress to SST anomalies in the eastern Pacific (Fig. S1—Supplementary material). The cluster analysis applied to historical and RCP8.5 simulations yields threshold values similar to the PI-control value. Sensitivity tests to this threshold value (taking an error of 5%) indicate that results presented in this paper are not impacted significantly. For a variation of  $\pm 5\%$  of the threshold, the number of strong El Niño events varies from 225 (–5.1%) to 262 (10.5%) for the historical simulations and from 271 (–10.3%) to 322 (6.6%) for the RCP8.5 simulations.

### 2.2.2 Extreme precipitation events

The definition follows that of Cai et al. (2014), that is based on the total DJF rainfall averaged over the Niño-3 region (150° W–90° W; 5° S–5° N). An extreme precipitation event is such that the rainfall index is above the threshold value of 5 mm/day. This definition was shown to be robust in accounting for changes in statistics of extreme events due to global warming despite the arbitrary choice of the threshold value in the warmer climate (Cai et al. 2017). Noteworthy, with such a definition, all extreme precipitation events are

however not necessarily associated with a strong or weak to moderate El Niño event. In particular, extreme precipitation events are defined from a threshold value of the DJF Niño-3 rainfall index. In that case, when two consecutive winters are affected by the same episode of anomalous positive surface temperature, causing precipitation events in DJF, the same warm episode is counted as two “independent El Niño events”. It thus allows two extreme precipitation events to take place from 1 year to another, while strong or weak-to-moderate El Niño events can last over more than 1 year (with the selected year corresponding to the maximum amplitude of the PC1 timeseries of the EOF analysis of SST anomalies). Nevertheless, with such a definition, 96% of the extreme precipitations events are concomitant with a strong El Niño event in the historical runs (Table 1). As will be seen, this percentage is reduced in the RCP8.5 runs (55%) due to both changes in the seasonality of strong El Niño events and the gradual warming of the eastern equatorial Pacific.

## 2.3 Heat budget

The equation of the SST change within the surface layer that is used for the heat budget is the following:

$$\left[\frac{\partial T'}{\partial t}\right] = - \left[u \frac{\partial T'}{\partial x}\right]' - \left[v \frac{\partial T'}{\partial y}\right]' - \left[w \frac{\partial T'}{\partial z}\right]' + \frac{Q'_{net}}{\rho_0 C_p h} + R' \quad (1)$$

The prime denotes the monthly anomaly relative to the mean climatology.  $T$  is the 4D-potential temperature,  $u$ ,  $v$  and  $w$  are respectively 4-D zonal, meridional and vertical currents. Square brackets indicate vertical integration over the surface layer, whose depth is set at 80 m. The first three right hand side terms correspond respectively to the zonal, meridional and vertical advectations. The term  $Q_{net}$  is the net ocean–atmosphere heat flux, including surface fluxes and penetrating short-wave radiation. The coefficients  $\rho_0$  and  $C_p$  are respectively the sea-water reference density ( $\text{kg/m}^3$ ) and the specific heat content ( $\text{J}/(\text{kg C})$ ). The residual term  $R$  includes the short-wave fluxes of heat out of the base of the mixed layer, the change in temperature associated with the freshwater flux, the horizontal and vertical diffusion of heat, and errors associated with the off-line calculation and the use of monthly mean outputs. The method further follows TD16 that consists in projecting the tendency terms of the SST equation (Eq. 1) onto the spatial patterns of the first two normalized EOF modes of the equatorial Pacific (2° S–2° N). The resulting timeseries are then linearly combined according to the definition of the E and C indices, which is convenient for inferring how processes contribute to the rate of change of SST anomalies in the E and C equatorial regions (Fig. 2). The projection of the heating rate onto the E mode is thus expressed as:

**Table 1** Statistics in El Niño events and extreme precipitation events

	Historical (1920–2005)			RCP8.5 (2006–2100)			Increase rate of frequency from present to future climate (%)
	Number of events	Frequency of occurrence (events/decade)	% of events concomitant with an extreme precipitation event/strong event (%)	Number of events	Frequency of occurrence (events/decade)	% of events concomitant with an extreme precipitation event/strong event (%)	
Number of strong events	237	0.65	59	302	0.77	89	+18.5
Number of moderate events	538	1.42	1 (5)	541	1.42	31 (167)	−0.1
Number of extreme precipitation events	146	0.39	96	489	1.26	55	+225.6
Number of strong events peaking in JAS	107	0.30	34	137	0.35	78	+16.5
Number of strong events peaking in ONDJ	120	0.33	79	44	0.11	100	−65.8
Number of strong events peaking in FMA	9	0.02	100	120	0.31	99	+1314.9

3682 (3800) years are considered for the historical (RCP8.5) runs. Note that the values of the frequency of occurrence have been rounded while the percentages in the text use the exact values

$$\left\langle \frac{\partial T'}{\partial t} \middle| E \right\rangle = \frac{1}{N_x N_y} \int_{120^\circ E}^{290^\circ E} \int_{2^\circ S}^{2^\circ N} \left( \frac{\partial T'}{\partial t}(x, y, t) \cdot E(x, y) \right) dx dy$$

This method has the advantage of objectively estimating the region of influence of the different feedbacks and their changes in a warmer climate, compared to the method where tendency terms are averaged over the classical Niño-4 (5° S–5° N, 160° E–210° E) and Niño-3 (5° S–5° N, 210° E–270° E) regions, or modified versions of them to take into account mean state biases in the CGCMs (Kug et al. 2010; Capotondi 2013; Stevenson et al. 2017). Since the E and C patterns are modified in the future climate (see Fig. 2 and Sect. 2.2.1), our method thus takes into account changes that may occur in the location of the main centers of the thermodynamical processes. To be able to compare the amplitude in the evolution of the tendency terms between the two climates, tendency terms for the RCP8.5 simulations are scaled by the projection coefficient of the RCP8.5 E and C patterns on their counterparts in the historical runs. The projection is done here over the domain (120° E–290° E; 2° S–2° N). The values of the scaling coefficient are equal to 1.18 (±10%) for both E and C modes over 2° S–2° N. The heat budget was calculated on the model native grid. The CESM uses the ocean POP model (Smith et al. 2010), which has a staggered Arakawa B-grid (Arakawa and Lamb 1977). The centered second-order finite differences scheme and

leap-frog time stepping were used for the calculation of the tendency terms following the model grid discretization.

### 3 Changes in Eastern Pacific El Niño events

#### 3.1 Composite evolution

As a first step, we present the composite evolution of the E and C indices during moderate and strong events in the two climates (Fig. 3). It indicates that, in this model, strong (moderate) El Niño events are preferentially of EP (CP) types because strong (moderate) El Niño events have large (weak) values of the E index. The E index during strong El Niño event tends also to peak from Aug(Y0), which is counterintuitive if compared to other historical indices (e.g. NINO34). This can be understood as follows: the E index accounts for SST variability in the far eastern Pacific where the thermocline is shallow and the thermocline feedback more intense than in the central equatorial Pacific. So when a Kelvin wave is triggered during the development of ENSO (typically during Feb–April Y(0)), the SST increase in the far eastern Pacific a couple month later, which projects on the E mode, then El Niño develops, which maintains an elevated E index. In other words, the first part of the warming in E is due to the forced Kelvin wave acting as a trigger of ENSO, while the second part of the warming in E is associated with the growing coupled mode. The values

of the C index are somewhat larger for moderate than for strong El Niños during the development phase. The C index has weaker positive values for strong El Niño events and can become negative during their decaying phase because strong El Niño events tend to be followed by La Niña events (DiNezio and Deser 2014), which the C index accounts for. The evolution of the indices is comparable to observations (see Fig. 4 of TD16) although the comparison is limited for strong El Niño events owing to their too few numbers in the observational record.

The striking feature of Fig. 3 is that the temporal evolution and amplitude of the indices do not change much from the present to the future climate in particular during the developing and mature phases of the El Niño composite, even if there are time frames when amplitude changes are statistically significant according to a Wilcoxon rank sum test. However, strong EP El Niño events last significantly longer by 2 months in the RCP8.5 simulations peaking in March (Y1) instead of December (Y0), while the central Pacific cools earlier and more than in the present climate. This suggests changes in seasonality of some events. Moderate El Niño events exhibit in general weaker changes in their evolution and amplitude, although there is a similar increase in persistence of the E index than that of strong events.

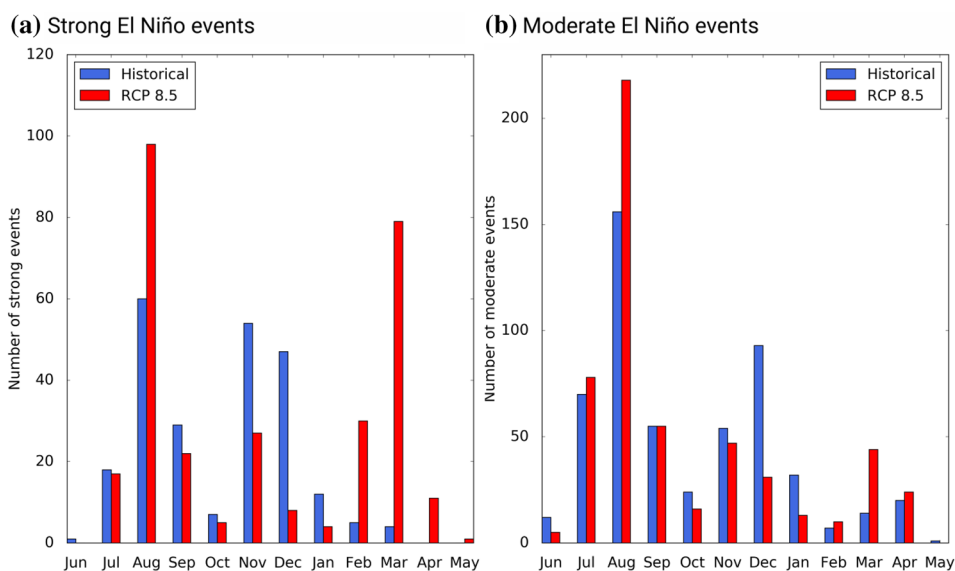
### 3.2 Seasonal stratification

In order to get further insights into the changes in ENSO statistics, the changes in the numbers of strong and moderate EP El Niño events are stratified according to the month of their peak value of the E index. Figure 4 allows identifying periods in the calendar year (hereafter referred to as “seasons”) when the number of events changes significantly from the historical to the RCP8.5 simulations. Considering periods

in the calendar year when the number of events is above 15 events for 3–4 consecutive months in the RCP8.5 simulations, three “seasons” can be defined: Jul–Aug–Sep (JAS), Oct–Nov–Dec–Jan (ONDJ) and Feb–Mar–Apr (FMA) (see Table 1). The threshold value of 15 events is selected arbitrarily and corresponds to 2% of the total number of events.

The results indicate a drastic change in the seasonal distribution of the number of events between the two climates. The most important changes are for strong EP El Niño events, with a significant increase (+1315%) in the number of events peaking during FMA. This is also observed for moderate EP El Niño events but to a lesser extent (+92%). Such a change indicates that, while the mean amplitude of EP El Niño event is weakly impacted by global warming (Fig. 3), this is not the case for the seasonal variance of the E index. This is evidenced in Fig. 5 that shows the climatological variance of the E index for the two climates. There is a significant increase in the E index variance (at the 95% confidence level based on a Wilcoxon test) at almost all calendar months, more pronounced for the FMA season (+40% increase in variance). The large increase in variance of the E index in FMA is likely to translate in a larger number of extreme precipitation events in the warmer climate because this corresponds to the season when the ITCZ has its southernmost position (Xie et al. 2018). In the CESM model, the frequency of occurrence of extreme precipitation events (see definition in Sect. 2.2) is projected to increase from 0.04 per 10 years (one event every 24.7 years) to 0.16 (one event every 6.4 years) on average over the last 50 years of the RCP8.5 simulations, which corresponds to a 3.9 fold increase of the number of extreme events at the end of the 21st century (+225% increase from the present to the future climate, Table 1). The CESM model thus projects more than a doubling of extreme precipitation events in the future

**Fig. 4** Number of **a** strong and **b** moderate El Niño events, defined from the E-index, as a function of the month in the calendar year when they peak (i.e. E index has maximum value) for (blue) historical and (red) RCP8.5 simulations. Note the different scale on the y axis between **a** and **b**





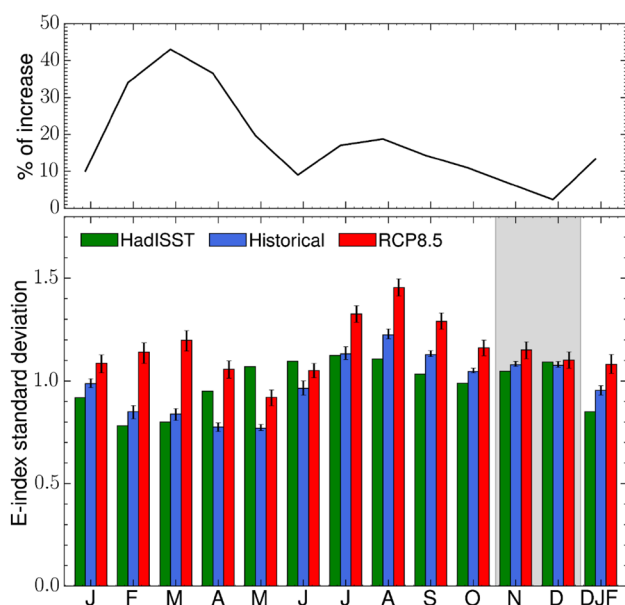


**Fig. 5** (Bottom panel) Climatological variance of the E index for (green) observations (1950–2017, 115° E–290° E; 10° S–10° N), (blue) the historical and (red) RCP8.5 simulations of CESM-LE. Error bars are inferred from the 95th and 5th percentiles of the distribution obtained by 10,000 realisations of randomly resampling the 40 (42) members and calculating their variance each time, any member being allowed to be selected again. (Top panel) Percentage of increase in variance from the historical to the RCP8.5 runs as a function of calendar month. The increase in variance between historical and RCP8.5 simulations is statistically significant at the 95% confidence level for all months except November and December (grey shading) according to Wilcoxon and bootstrap tests. The increase in variance associated with the DJF mean is provided on the right hand side of each panel. It is significant at the 95% confidence level

climate, consistent with Cai et al. (2014). The CESM model exhibits however a more modest increase, from the present to the warmer climate, in the number of strong EP El Niño events than in the number of extreme precipitation events. In particular, the number of strong EP El Niño events (extreme precipitation events) increases from 237 (146) in the historical period to 302 (489) in the RCP8.5 period, which corresponds to an increase of their frequency of occurrence (in events/decade) of +18% from the present to the future climate (Table 1), so that the increase in strong EP El Niño events is much less than the increase in extreme precipitation events. This can be interpreted broadly as resulting from the fact that moderate EP El Niño events can yield extreme precipitation events in the warmer climate due to increased mean SST in the eastern equatorial Pacific (Cai et al. 2014), independently of whether or not the moderate EP El Niño events undergo a change in their dynamics. However, since the overall number of (strong and moderate) EP El Niño events has almost no change (not shown), the 18% increase in the frequency of strong EP El Niño events indicates that global warming may favor the “high-regime” of ENSO

(TD16), suggesting that the increase in extreme precipitation events in the warmer climate does not solely result from the warming of the cold tongue (Cai et al. 2014). This will be further documented in the discussion section. In the following, we investigate the processes explaining the increased persistence of EP El Niño and the emergence of events peaking in FMA in the warmer climate, focusing on key ENSO oceanic processes sensitive to the increased vertical stratification, i.e. the thermocline feedback and the recharge of heat content.

## 4 ENSO processes and increased stratification

In this section, the focus is on the processes that could explain the increased variance and persistence of the E index in FMA. As mentioned in the introduction, the increase in vertical stratification is a salient feature of the climate change pattern on temperature in the ocean, which has implications for ENSO dynamics. Not only it modulates the thermocline feedback through changing the relationship between SST and thermocline depth fluctuations (Dewitte et al. 2012), but it can also influence the dynamical response of the ocean through the projection of momentum forcing on the wave dynamics (Philander 1978; Dewitte 2000), and thereby the ENSO stability (Yeh et al. 2010; Thual et al. 2011, 2013). Recently Cai et al. (2018) showed that changes in vertical stratification due to greenhouse warming are associated with the increase in variance of the EP El Niño events in an ensemble composed of models simulating ENSO diversity/non-linearity similar to that of CESM (see Sect. 2). We thus here use the CESM simulations to get insights in the mechanisms at work for explaining the increased climatological variance in strong EP El Niño events.

### 4.1 Recharge-discharge process

Heat content along the equator is a precursor of ENSO and its primary source of predictability, which has been conceptualized by the recharge-discharge oscillator model (Jin 1997). Although large heat content anomalies are not always necessary for strong EP El Niño to occur (TD16), it is worth diagnosing the recharge-discharge process in the model, as it can explain to some extent the persistence of SST anomalies during ENSO. In the framework of the simple recharge-discharge model (Jin 1997), a stronger recharge would imply a longer lasting El Niño event once it has developed. Figure 6 shows the strong El Niño composite evolution of estimates of the so-called tilt and warm water volume (WWV) modes that depict the recharge-discharge-discharge process (Clarke 2010). The WWV mode is phase-shifted (ahead by ~6 months) with the tilt mode that

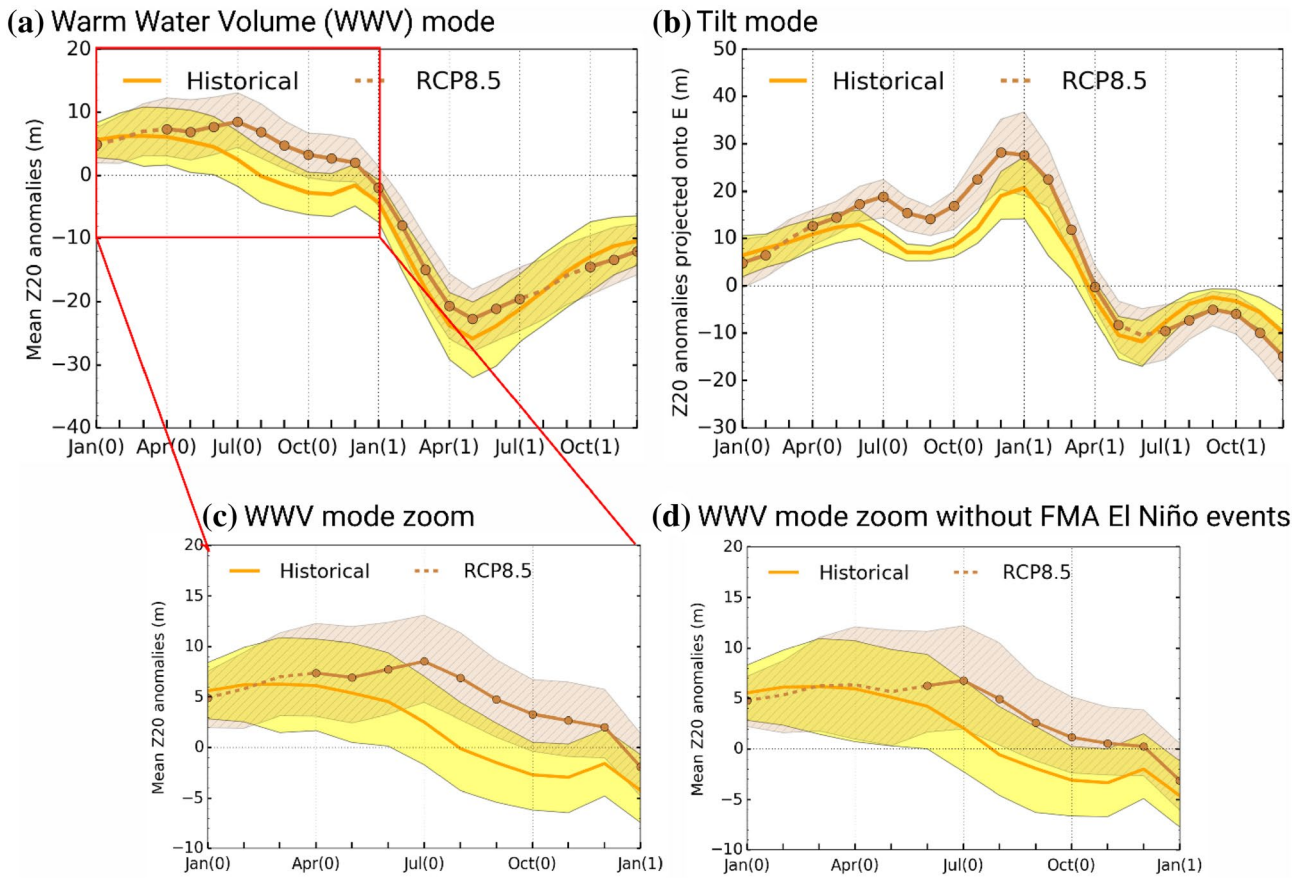


**Fig. 6** (Top panels) Composite evolution of **a** the Warm water volume (WWV) mode and **b** the tilt mode during strong El Niño events for the (solid yellow lines) historical and (brown lines with dots) RCP8.5 runs. The WWV mode corresponds to the mean 20 °C isotherm depth (Z20) anomalies (m) averaged over the region (115°–290° E; 2° S–2° N). The tilt mode is estimated by projecting the 20 °C isotherm depth (Z20) anomalies (m) onto the E mode pattern calculated over the domain (115° E–290° E; 2° S–2° N). The shaded

ing indicates the range of values between the 25th and 75th percentiles of the distribution of the members. The portions of the curves in dashed line for the RCP8.5 composites indicate when the changes between historical and RCP8.5 are not significant at 95% confidence level based on a Wilcoxon rank sum test. (Bottom panels) Composite evolution of Warm water volume (WWV) over Jan (Y0)–Jan(Y1) for **c** all the strong El Niño events, and **d** excluding the contribution of strong El Niño events peaking in FMA

accounts for the quasi-instantaneous response of the eastern Pacific thermocline to wind stress anomalies. It is clear from Fig. 6a that the recharge process is increased in the warmer climate (the mean over the period Jun(Y0)–Oct(Y0) increases from 0.55 to 6.25 m between the two climates), while the tilt mode amplitude also increases prior to the ENSO peak (Fig. 6b). The tilt mode amplitude increase is consistent with westerly winds projecting more on the ocean dynamics in the warmer climate due to the increased stratification in the central Pacific (Fig. 7) (Dewitte et al. 1999; Thual et al. 2011). Note that it was checked that the zonal equatorial wind stress integrated from one side of the Pacific to the other (that represents an estimate of the tilt mode which does take explicitly into account the change in stratification) during the EP El Niño events is not significantly changed between the two climates (not shown) so that the increase in the amplitude of the tilt mode is not

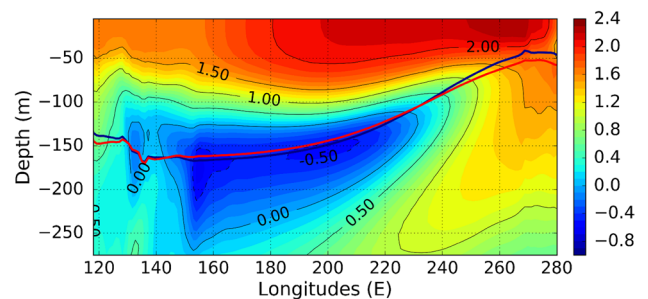


**Fig. 7** Mean differences of equatorial (2° S–2° N) temperature (in °C) between the RCP8.5 and historical simulations. The blue (red) line indicates the mean depth of the 20 °C isotherm for the historical (RCP8.5) simulations

the result of changes in the amplitude of wind stress forcing that contributes to the build-up of heat content, but instead has to result from the fact that wind stress forcing projects more efficiently onto wave dynamics due to the increased stratification. The increase lasts until Jan(Y1) so that the effect on SST anomalies could last until ~ Mar(Y1) through the thermocline feedback because of the delayed response of SST anomalies to thermocline fluctuations (Zelle et al. 2004; see also Sect. 4.2). Regarding the WWV mode, the change in amplitude in Jul(Y0)–Oct(Y0) from the present to the future climate is certainly more difficult to interpret because of likely compensating effects amongst different processes (Thual et al. 2011; Lengaigne et al. 2012; Izumo et al. 2018), the potential role of changes in off-equatorial high-frequency winds (McGregor et al. 2016; Neske and McGregor 2018) and other sources of external forcing (see Sect. 5). However, the increase in amplitude of the WWV can be associated to a large extent with the increased occurrence of the strong events peaking in FMA as evidenced by the composite of the WWV evolution with and without strong events peaking in FMA (Fig. 6c, d). The increase in amplitude of the WWV is statistically significant (at 95% confidence level based on a Wilcoxon rank sum test) from Apr(Y0) to Jan(Y1) when considering the events peaking in FMA. The increase is statistically significant only from Jun(Y0) when El Niño events whose peak occurs in FMA are not considered. Note that the same diagnosis was done using the thermocline depth, i.e. the depth of the maximal vertical temperature gradient. While the change with global warming of the WWB amplitude prior to the ENSO peak (i.e. Jun(Y0)–Oct(Y0)) is less pronounced, it is statistically significant when considering strong El Niño events peaking in FMA (not shown).

## 4.2 Mixed-layer processes

While the strengthened vertical stratification increases the effectiveness of momentum flux onto the wave dynamics (Dewitte et al. 1999), which tends to destabilize ENSO by increasing the coupling efficiency between the ocean and the atmosphere (Thual et al. 2011, 2013), the sensitivity of ENSO to changes in stratification also operates through changes in the mixed-layer processes. Owing to the shallow thermocline in the eastern Pacific, the main oceanic process there is the mean vertical advection of anomalous temperature  $(-\bar{w} \cdot \frac{\partial T'}{\partial z})$ , often referred to as the thermocline feedback (An and Jin 2001). Since changes in the thermocline feedback not only depend on changes in the magnitude of the seasonal upwelling rate ( $\bar{w}$ ) but also on changes in the vertical gradient of anomalous temperature between the surface and the base of the mixed layer  $(\frac{\partial T'}{\partial z})$ , inferring its sensitivity to vertical stratification is not straightforward. In

particular, increased stratification in the eastern Pacific may reduce the effectiveness of upwelling through flattening and tightening the isotherms, while it could increase the sensitivity of SST anomalies to thermocline fluctuations through enhancing mean vertical diffusivity (Zelle et al. 2004). Compensating effects are thus possible.

As a first step, we present the composite evolution during strong El Niño events in the eastern Pacific (E region) of the mixed-layer processes (tendency terms) for the present and future climates (Fig. 8). For conciseness sake, we focus hereafter on the developing and peak phases, noting also that the residual term being relatively large during the decaying phase (Fig. 8e), the interpretation of the results is not straightforward during that particular phase. As expected, total vertical advection exhibits the largest amplitude (Fig. 8d). It was checked through a Reynolds decomposition of the tendency terms that the main contributor to total vertical advection is the thermocline feedback, with non-linear vertical advection and anomalous vertical advection of mean temperature (“upwelling feedback”) only marginally contributing during the onset and peak phase of strong EP El Niño events (Fig. S2—Supplementary material) consistently with TD16. The residual term has a comparable contribution (cooling) than the thermal damping term, and can be interpreted as resulting from the reduced vertical diffusivity in the first 80 m as the mixed-layer deepens. The largest changes between the present and future climates are for vertical advection and thermal damping with a 71% increase (90% reduction) for the average over Apr(Y0)–Feb(Y1) for vertical advection (thermal damping) relatively to the value over the present climate (Fig. 8f). Changes in these two opposite sign terms explain why the rate of SST change is hardly impacted from the present climate to the future climate. While the larger contribution of thermal damping is expected from the increase variance of the E index from the present to the future climate, the increase in the magnitude of vertical advection is more difficult to interpret. 77% of this increase is associated with the contribution of climatological vertical advection of anomalous temperature (Fig. S2), so that it can be interpreted as resulting from the combined effects of the weakening of the Walker circulation on the seasonal upwelling on the one hand (DiNezio et al. 2009; Dewitte et al. 2012; Chung et al. 2019) and of the increased stratification on the relationship between SST and thermocline anomalies on the other hand. Figures 9a, b present estimates of the changes of these two quantities (i.e. upwelling rate and the slope of the linear relationship between SST and thermocline anomalies) between the two climates. The slope of the linear relationship between SST and thermocline anomalies is estimated for lag between –6 and 6 months and the maximum value is shown considering that temperature anomalies in the vicinity of the thermocline are transported to the surface by a combination of

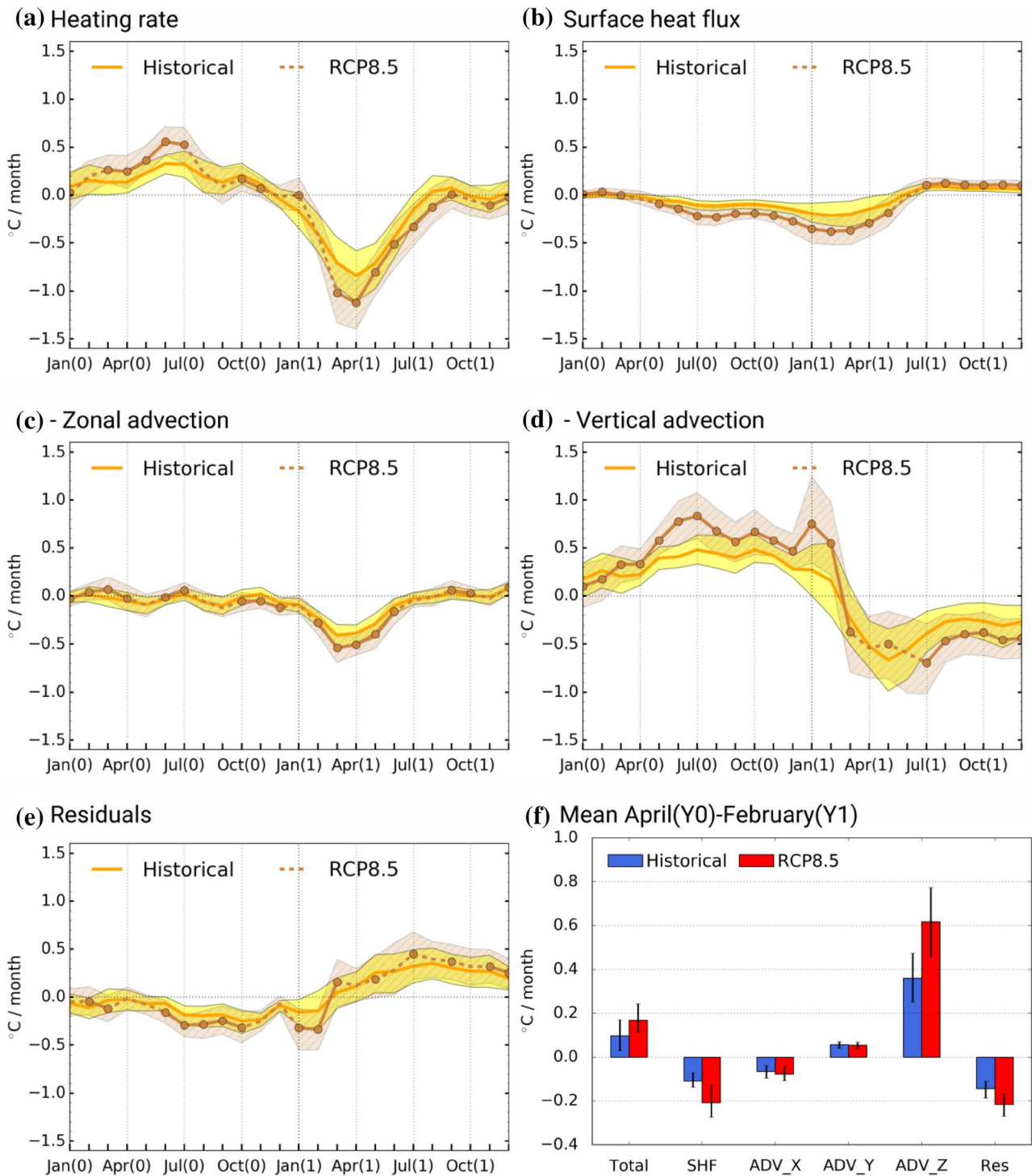


**Fig. 8** Heat budget projected onto the E mode: composite evolution during strong El Niño events for **a** the total heating rate, **b** the surface net heat flux, **c** the zonal advection, **d** the vertical advection and **e** the residuals (i.e. difference between the rate of SST change and all tendency terms including meridional advection) for the (yellow) historical and (brown) RCP8.5 simulations. All terms are projected onto the E mode patterns (see the method section). The shading indicates the range of values between the 25th and 75th percentiles of the distribu-

tion of the members. The portions of the curves in dashed line for the RCP8.5 composites indicate when the changes between historical and RCP8.5 are not significant at 95% confidence level based on a Wilcoxon rank sum test. **f** Mean values over the period Apr(Y0)–Feb(Y1) of all the terms. Error bars are inferred from the 95th and 5th percentiles of the distribution obtained by randomly resampling the values of tendency terms of the 40 (42) members, any members being allowed to be selected again

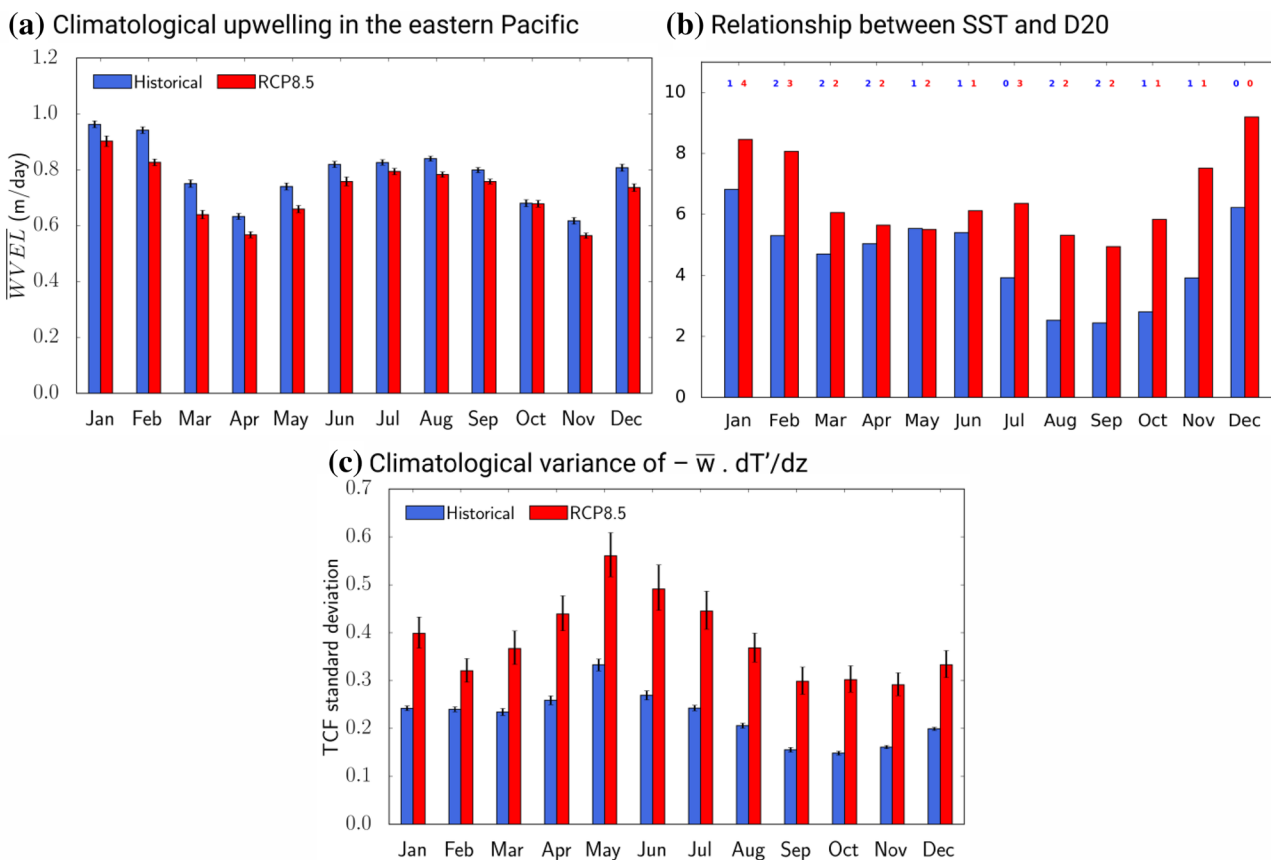


**Fig. 9** **a** Changes in climatological mean upwelling in the eastern Pacific (Niño-3 region) for the (blue) historical and (red) RCP8.5 simulations (m/day). Error bars correspond to the inter-members spread (standard deviation). **b** Changes in the maximum value of the slope of the lagged relationship between SST anomalies (E index) and the depth of the 20 °C isotherm (D20) anomalies in the eastern Pacific (projected onto the E mode) for the (blue) historical and (red) RCP8.5 simulations. The lag is indicated above the corresponding

bars (positive value corresponds to D20 ahead SST). **c** Climatological variance of the thermocline feedback for the (blue) historical and (red) RCP8.5 simulations (°C/days). Error bars are inferred from the 95th and 5th percentiles of the distribution obtained by 10,000 realizations of randomly resampling the 40 (42) members and calculating their variance each time, any member being allowed to be selected again

upwelling and vertical mixing, which introduces a delay in the time dependence of the local relation between SST and thermocline anomalies (Zelle et al. 2004). As expected, the climatological upwelling rate is reduced in the warmer climate (Fig. 9a). The reduction is most important in boreal winter reaching -14% in March. The decrease is statistically significant at the 95% confidence level except for the month of October. On the other hand, the sensitivity of the SST to thermocline fluctuations is significantly increased in particular with a maximum relative increase in August (+100%). On average over the year, the relationship between SST and thermocline fluctuations is increased by 46%. Such increase largely compensates for the decrease in climatological upwelling and yield an overall increase in the thermocline feedback as evidenced by Fig. 9c that shows the change in climatological variance of the mean vertical advection of anomalous temperature between the present and the future climate. In particular, the relative increase in variance is

maximum in May–June–July (+83%), which corresponds to the season when the tropical Pacific system becomes highly unstable (Stein et al. 2010) and is more susceptible to develop an El Niño event. As a summary, Fig. 8f presents the averaged changes in amplitude of the tendency terms during the developing phase of strong EP El Niño events. The largest increase is for vertical advection (+71%), 77% of which is attributed to the thermocline feedback.

### 5 Discussions and concluding remarks

We have investigated the sensitivity of ENSO dynamics to mean state changes in a model that has skill in simulating ENSO diversity and non-linearity. We find that, in the CESM model, the persistence of strong EP events is increased by 2 months so that the variance in SST anomalies in the eastern Pacific is significantly increased over the

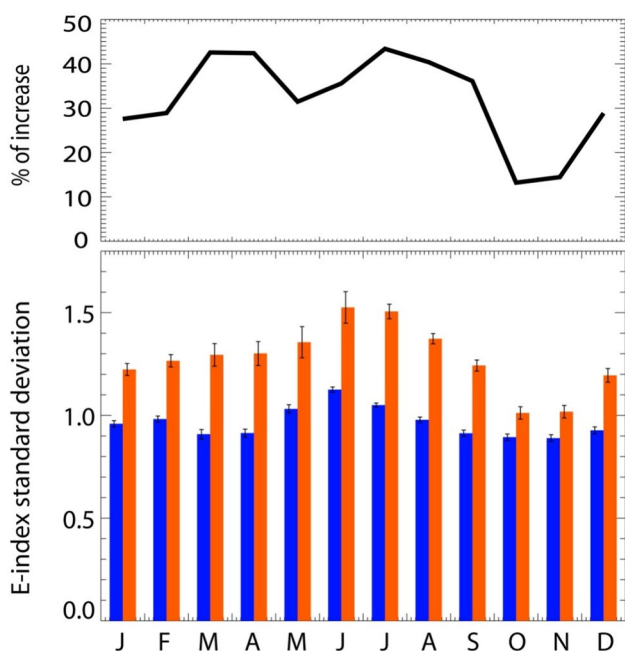


**Fig. 10** (Bottom panel) Climatological variance of the E-index for (blue) the historical and (red) RCP8.5 simulations of an ensemble of CMIP5 models. The ensemble corresponds to the 17 models used in Cai et al. (2018) that realistically represent the nonlinear Bjerknes feedback. Error bars are inferred from the standard deviation of 10,000 realisations obtained by randomly resampling the 17 models and calculating their variance each time, any models being allowed to be selected again. (Top panel) Percentage of increase in variance from the historical to the RCP8.5 runs as a function of calendar month

FMA season when the ITCZ is about to reach its southernmost position. Noteworthy a similar behavior is found in the CMIP5 ensemble (Fig. 10), allowing to some extent to generalize the results obtained here from the CESM model.

While recent studies have shown that the number of extreme precipitation events associated with El Niño is projected to increase in the warmer climate (Cai et al. 2014, 2015b), the mechanisms by which this will take place remain unclear. Here we suggest that a portion of the increase in extreme precipitation events in the warmer climate is associated with the increase in the number of strong EP El Niño events, in particular those that peak in FMA, which corresponds to the season when climatological SST in the eastern Pacific is already high. Those events are thus strongly coupled to the ITCZ and do not necessarily require the anthropologically-forced mean SST warming trend in the eastern Pacific to yield extreme precipitation events. In order to estimate the proportion of extreme precipitation events that relates either to moderate or strong El Niño events, we consider the number of events over 10-year running windows among all simulation members (i.e. at least 400 years are considered for each chunk) and estimate the proportion of El Niño events (strong and moderate) compositing extreme precipitation events along historical and RCP8.5 periods (Fig. 11). The increase (by 1315%) in the frequency of occurrence of strong EP El Niño events peaking in FMA explains 24% of the increase in the frequency of occurrence of extreme precipitation events in the CESM model. 9% and 21% of the increase in the frequency of occurrence of extreme precipitation events are explained by the frequency of occurrence of strong El Niño events peaking in ONDJ

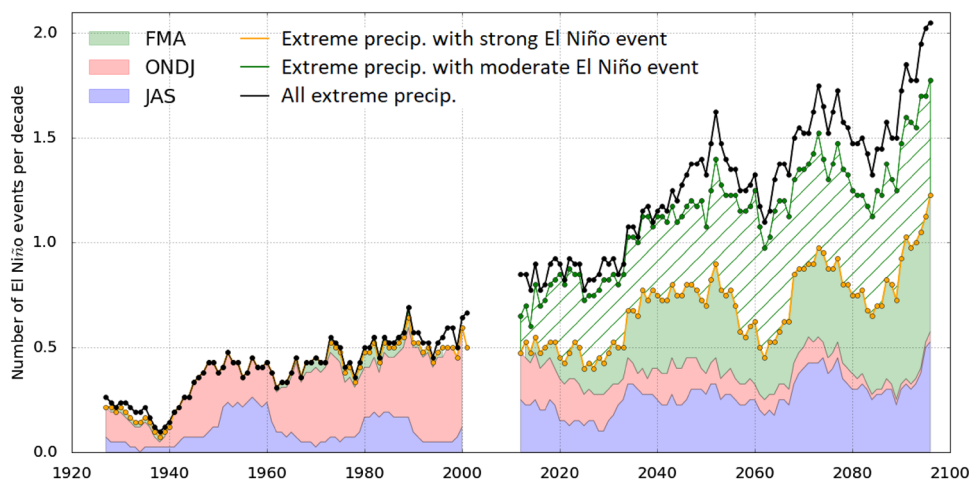


**Fig. 11** Number of extreme precipitation events over 10-year running windows that are concomitant with either strong or moderate El Niño events among the ensemble of the historical (1920–2005) and the RCP8.5 (2006–2100) simulations. Hatch indicates the proportion of moderate El Niño events while shading is for strong El Niño events. The colors refer to the seasons as defined in Sect. 3.2: blue for

JAS events, red for ONDJ events and green for FMA events. Note that there is a little share of extreme events that are not concomitant with either a moderate or a strong El Niño events (i.e. the green curve does not overlap the black curve), which is due to internal variability in precipitation (year of extreme precipitation event without an El Niño event)

and JAS respectively (see Sect. 3.2 for the definition of “seasons”). This sums to 54% of the increase in the frequency of occurrence of extreme precipitation events thus explained by the increase in the frequency of occurrence of strong El Niño events. Concomitantly, the increased proportion of extreme precipitation events associated with weak and moderate El Niño events (which represents an additional 0.43 events/decade of weak to moderate El Niño events that relates to an extreme precipitation events in the warmer climate) results in that 34% of the increase in extreme precipitation events are associated with moderate El Niño events and thus due to the warmer mean SST in the eastern equatorial Pacific. Note that in the present climate, there is almost no weak to moderate El Niño event (i.e. 0.003 events/decade) that relates to extreme precipitation events (versus 0.43 events/decades in the future climate). The remaining 12% of the increase in the frequency of occurrence of extreme precipitation events could not be explained by the occurrence of an El Niño event and thus corresponds to internal variability in precipitation in a warmer climate. Overall Fig. 11 illustrates the influence of the number of events peaking in FMA on the change in extreme precipitation events in the warmer climate, although very few of these events (9) exist in the historical simulation. It indicates that changes in the statistics of extreme precipitation events cannot be solely attributed to changes in mean SST in the equatorial eastern Pacific i.e. the warmer mean SST becoming closer to the convective threshold, but also depend on changes in ENSO dynamics.

The “emergence” of strong EP El Niño peaking in FMA in the warmer climate is suggested to be associated with the increased vertical stratification across the equatorial Pacific, a salient feature of the climate change patterns in climate models (Yeh et al. 2009a, b; DiNezio et al. 2009; Cai et al. 2018). Cai et al. (2018) showed in particular that the increased variance in Eastern Pacific SST anomalies is associated with the increase in vertical stratification. We suggest further that the increased persistence of EP El Niño events is resulting from both a stronger recharge process and a more effective thermocline feedback in the warming climate due to an increased vertical stratification. In particular, the sensitivity of SST anomalies in the far eastern Pacific to thermocline fluctuations is significantly increased in FMA and overwhelms the reduction in mean upwelling (Fig. 9). The recharge process is also shown to be enhanced in the warmer climate, which can be interpreted as resulting from the increased stratification in the central-western Pacific where wind stress can be more efficiently projected onto the wave dynamics. Overall our study suggests that the influence of the increased ocean vertical stratification in a warmer climate on ENSO could be understood in terms of two main mechanisms involving mostly linear processes, i.e. (1) on the dynamical side, a stronger recharge process and an overall more energized wave dynamics, and (2) on

the thermodynamical side, an increased thermocline feedback in the eastern Pacific. These processes work together to produce the increased persistence/variance in EP El Niño events in the warmer climate.

Of course, considering the coupled nature of ENSO, there are other potentially important processes that could be at play to explain the longer duration of strong EP El Niño events in the warmer climate and their changing seasonal stratification. In particular, non-linear oceanic processes are important for the strong El Niño regime (Jin et al. 2003) although non-linear advection, the main contributor to the oceanic non-linearities during ENSO, does not appear essential for the onset of strong EP El Niño events (TD16), a feature that is also observed here (Fig. S2c). Nevertheless non-linear advection is increased by 120% from the present to the future climate, over Apr-May-Jun(Y1), the period over which it peaks in the E region, contributing to the longer persistence of warm anomalies during strong El Niño events. Determining if such increase is related to the increase in vertical stratification would deserve further investigation which is beyond the scope of the present study considering the likely interplay between the various non-linear processes. The other important non-linear processes for ENSO are those encapsulated in the Bjerknes feedback and are atmospheric processes by nature (Dommenget et al. 2013, TD16). While the details of the change in the characteristics of the Bjerknes feedback is beyond the scope of the present study, we note that, within the approximations of our methodological approach, the slopes of the piecewise linear relationship between the E index and the zonal wind stress in the eastern equatorial Pacific are weakly changed from the present to the future climate (See Figure S1). This suggests that the characteristics of the Bjerknes feedback are not fundamentally modified in this model from the present to the future climate, although the convective SST anomaly threshold appears to have changed consistently with Johnson and Xie (2010) that showed that it is not absolute and varies with the mean climate (e.g. the temperature of the free troposphere). The other key ingredient for strong El Niño events to develop, that was not looked at here although it can non-linearly interact with the equatorial ENSO dynamics, is the nature of the changes in the external stochastic forcing that has multiple facets. While high-frequency stochastic forcing, in the form of Westerly Wind Bursts (WWBs), is expected to energize more wave dynamics in the warmer climate, it is not clear how its characteristics will change in the future (Bui and Maloney 2018; Maloney et al. 2019). We note here that, in the CESM model, the high-frequency (frequency  $> 90$  days<sup>-1</sup>) variance of the equatorial zonal wind stress is increased from the present to the future climate (not shown), which could contribute to the stronger recharge process in the warmer climate for strong El Niño events (see Fig. 6). This would deserve further investigation

which is planned for future work. In particular, since there is more and more evidence that the low-frequency component of the external forcing to ENSO is certainly as important as the high-frequency component (Dommenges and Yu 2017; Takahashi et al. 2018), such investigation will have to consider all aspects of the external forcing, including the North Pacific Meridional Mode (Chiang and Vimont 2004) that is also suggested to become more energetic in the warmer climate in this model (Liguori and Di Lorenzo 2018).

**Acknowledgements** We acknowledge the CESM Large Ensemble Community Project for providing model outputs, which are available on <https://www.earthsystemgrid.org>. The CESM project is supported by the National Science Foundation and the Office of Science (BER) of the US Department of Energy. B. Dewitte acknowledges supports from FONDECYT (projects 1171861 and 1190276) and the Agence Nationale de la Recherche (ANR, project ARISE). A. Capotondi was supported by the NASA Physical Oceanography Program (Award NNX15AG46G). S.-W. Yeh was supported by National Research Foundation Grant NRF-2018R1A5A1024958.

## References

- An S-I, Jin F-F (2001) Collective role of thermocline and zonal advective feedbacks in the ENSO mode. *J Clim* 14:3421–3432
- Arakawa A, VR Lamb (1977) Computational design of the basic dynamical processes of the UCLA general circulation model. methods in computational physics: advances in research and applications. In: J Chang ed, Elsevier, volume 17 of general circulation models of the atmosphere, pp 173–265
- Barber RT, Chavez FP (1983) Biological consequences of El Niño. *Science* 222:1203–1210. <https://doi.org/10.1126/science.222.4629.1203>
- Bayr T, Wengel C, Latif M, Dommenges D, Lübbecke J, Park W (2018) Error compensation of ENSO atmospheric feedbacks in climate models and its influence on simulated ENSO dynamics. *Clim Dyn*. <https://doi.org/10.1007/s00382-018-4575-7>
- Bellenger H, Guilyardi E, Leloup J, Lengaigne M, Vialard J (2014) ENSO representation in climate models: from CMIP3 to CMIP5. *Clim Dyn* 42:1999–2018. <https://doi.org/10.1007/s00382-013-1783-z>
- Bui HX, Maloney ED (2018) Changes in Madden-Julian oscillation precipitation and wind variance under global warming. *Geophys Res Lett* 45:7148–7155
- Cai W, Borlace S, Lengaigne M, van Rensch P, Collins M, Vecchi G, Timmermann A, Santoso A, McPhaden MJ, Wu L, England MH, Wang G, Guilyardi E, Jin F-F (2014) Increasing frequency of extreme El Niño events due to greenhouse warming. *Nature Clim Change* 4:111–116
- Cai W, Santoso A, Wang G, Yeh S-W, An S-I, Cobb KM, Collins M, Guilyardi E, Jin F-F, Kug J-S, Lengaigne M, McPhaden MJ, Takahashi K, Timmermann A, Vecchi G, Watanabe M, Wu L (2015a) ENSO and greenhouse warming. *Nature Clim Change* 5:849–859. <https://doi.org/10.1038/nclimate2743>
- Cai W, Wang G, Santoso A, McPhaden MJ, Wu L, Jin F-F, Timmermann A, Collins M, Vecchi G, Lengaigne M, England MH, Dommenges D, Takahashi K, Guilyardi E (2015b) Increased frequency of extreme La Niña events under greenhouse warming. *Nature Clim Change* 5:132–137. <https://doi.org/10.1038/nclimate2492>
- Cai W, Wang G, Santoso A, Lin X, Wu L (2017) Definition of extreme El Niño and its impact on projected increase in extreme El Niño frequency. *Geophys Res Lett*. <https://doi.org/10.1002/2017GL075635>
- Cai W, Wang G, Dewitte B, Wu L, Santoso A, Takahashi K, Yang Y, Carréric A, McPhaden MJ (2018) Increased variability of eastern Pacific El Niño under greenhouse warming. *Nature* 564:201–206. <https://doi.org/10.1038/s41586-018-0776-9>
- Capotondi A (2013) ENSO diversity in the NCAR CCSM4 climate model. *J Geophys Res Oceans* 118:4755–4770. <https://doi.org/10.1002/jgrc.20335>
- Capotondi A, Alexander MA, Bond NA, Curchitser EN, Scott JD (2012) Enhanced upper-ocean stratification with climate change in the CMIP3 models. *J Geophys Res* 117:C04031. <https://doi.org/10.1029/2011JC007409>
- Capotondi A, Wittenberg AT, Newman M, Di Lorenzo E, Yu J-Y, Braconnot P, Cole J, Dewitte B, Giese B, Guilyardi E, Jin F-F, Karnauskas K, Kirtman B, Lee T, Schneider N, Xue Y, Yeh S-W (2015) Understanding ENSO diversity. *Bull Am Meteor Soc* 96:921–938. <https://doi.org/10.1175/BAMS-D-13-00117.1>
- Carr ME, Strub PT, Thomas AC, Blanco JL (2002) Evolution of 1996–1999 La Niña and El Niño conditions off the western coast of South America: a remote sensing perspective. *J Geophys Res* 107(C12):3236. <https://doi.org/10.1029/2001JC001183>
- Chiang JCH, Vimont DJ (2004) Analogous Pacific and Atlantic meridional modes of tropical atmosphere-ocean variability. *J Clim* 17:4143–4158. <https://doi.org/10.1175/JCLI4953.1>
- Choi J, An S-I, Yeh S-W (2012) Decadal amplitude modulation of two types of ENSO and its relationship with the mean state. *Clim Dyn* 38:2631–2644. <https://doi.org/10.1007/s00382-011-1186-y>
- Clarke AJ (2010) Analytical theory for the quasi-steady and low-frequency equatorial ocean response to wind forcing: the “tilt” and “warm water volume” modes. *J Phys Oceanogr* 40:121–137. <https://doi.org/10.1175/2009JPO4263.1>
- Deser C, Phillips AS, Tomas RA, Okumura YM, Alexander MA, Capotondi A, Scott JD, Kwon Y-O, Ohba M (2012) ENSO and Pacific decadal variability in the community climate system model version 4. *J Clim* 25:2622–2651. <https://doi.org/10.1175/JCLI-D-11-00301.1>
- Dewitte B (2000) Sensitivity of an intermediate ocean-atmosphere coupled model of the tropical Pacific to its oceanic vertical structure. *J Clim* 13:2363–2388. [https://doi.org/10.1175/1520-0442\(2000\)013%3c2363:SOAIOA%3e2.0.CO;2](https://doi.org/10.1175/1520-0442(2000)013%3c2363:SOAIOA%3e2.0.CO;2)
- Dewitte B, Takahashi K (2017) Diversity of moderate El Niño events evolution: role of air–sea interactions in the eastern tropical Pacific. *Clim Dyn*. <https://doi.org/10.1007/s00382-017-4051-9>
- Dewitte B, Reverdin G, Maes C (1999) Vertical structure of an OGCM simulation of the equatorial Pacific Ocean in 1985–1994. *J Phys Oceanogr* 29(7):1542–1570
- Dewitte B, Cibot C, Périgaud C, An S-I, Terray L (2007) Interaction between near-annual and ENSO modes in a CGCM simulation: role of the equatorial background mean state. *J Clim* 20:1035–1052. <https://doi.org/10.1175/JCLI4060.1>
- Dewitte B, Thual S, Yeh S-W, An S-I, Moon B-K, Giese BS (2009) Low-frequency variability of temperature in the vicinity of the equatorial Pacific thermocline in SODA: role of equatorial wave dynamics and ENSO asymmetry. *J Clim* 22:5783–5795. <https://doi.org/10.1175/2009JCLI2764.1>
- Dewitte B, Choi J, An S-I, Thual S (2012) Vertical structure variability and equatorial waves during central Pacific and eastern Pacific El Niños in a coupled general circulation model. *Clim Dyn* 38:2275–2289. <https://doi.org/10.1007/s00382-011-1215-x>
- DiNezio PN, Deser C (2014) Nonlinear Controls on the persistence of La Niña. *J Clim* 27:7335–7355. <https://doi.org/10.1175/JCLI-D-14-00033.1>
- DiNezio PN, Clement AC, Vecchi GA, Soden BJ, Kirtman BP, Lee SK (2009) Climate response of the equatorial Pacific to global warming. *J Clim* 22:4873–4892. <https://doi.org/10.1175/2009JCLI2982.1>



- Dommenget D, Yu Y (2017) The effects of remote SST forcings on ENSO dynamics, variability and diversity. *Clim Dyn* 49:2605–2624. <https://doi.org/10.1007/s00382-016-3472-1>
- Dommenget D, Bayr T, Frauen C (2013) Analysis of the non-linearity in the pattern and time evolution of El Niño southern oscillation. *Clim Dyn* 40:2825–2847. <https://doi.org/10.1007/s00382-012-1475-0>
- Gent PR, Danabasoglu G, Donner LJ, Holland MM, Hunke EC, Jayne SR, Lawrence DM, Neale RB, Rasch PJ, Vertenstein M, Worley PH, Yang Z-L, Zhang M (2011) The community climate system model version 4. *J Clim* 24:4973–4991. <https://doi.org/10.1175/2011JCLI4083.1>
- Graham FS, Wittenberg AT, Brown JN, Marsland SJ, Holbrook NJ (2017) Understanding the double peaked El Niño in coupled GCMs. *Clim Dyn* 48:2045–2063. <https://doi.org/10.1007/s00382-016-3189-1>
- Ham Y-G, Kug J-S (2012) How well do current climate models simulate two types of El Niño? *Clim Dyn* 39:383–398. <https://doi.org/10.1007/s00382-011-1157-3>
- Hunke EC, Lipscomb W (2010) CICE: the Los Alamos sea ice model documentation and software user's manual version 4.0 LA-CC-06-012. In: Tech. Rep. LA-CC-06-012
- Hurrell JW, Holland MM, Gent PR, Ghan S, Kay JE, Kushner PJ, Lamarque J-F, Large WG, Lawrence D, Lindsay K, Lipscomb WH, Long MC, Mahowald N, Marsh DR, Neale RB, Rasch P, Vavrus S, Vertenstein M, Bader D, Collins WD, Hack JJ, Kiehl J, Marshall S (2013) The community earth system model: a framework for collaborative research. *Bull Am Meteor Soc* 94:1339–1360. <https://doi.org/10.1175/BAMS-D-12-00121.1>
- Hwang Y-T, Frierson DMW (2013) Link between the double-intertropical convergence zone problem and cloud biases over the Southern Ocean. *PNAS*. <https://doi.org/10.1073/pnas.1213302110>
- Izumo T, Lengaigne M, Vialard J, Suresh I, Planton Y (2018) On the physical interpretation of the lead relation between Warm Water Volume and the El Niño Southern Oscillation. *Clim Dyn*. <https://doi.org/10.1007/s00382-018-4313-1>
- Jin F-F (1997) An equatorial ocean recharge paradigm for ENSO. Part I: conceptual model. *J Atmos Sci* 54:811–829. [https://doi.org/10.1175/1520-0469\(1997\)054%3c0811:AEORP%3e2.0.CO;2](https://doi.org/10.1175/1520-0469(1997)054%3c0811:AEORP%3e2.0.CO;2)
- Jin F-F, An SI, Timmermann A, Zhao J (2003) Strong El Niño events and nonlinear dynamical heating. *Geophys Res Lett* 30:20-1. <https://doi.org/10.1029/2002gl016356>
- Johnson NC, Xie S-P (2010) Changes in the sea surface temperature threshold for tropical convection. *Nat Geosci* 3:842–845. <https://doi.org/10.1038/ngeo1008>
- Karamperidou C, Jin F-F, Conroy JL (2017) The importance of ENSO nonlinearities in tropical pacific response to external forcing. *Clim Dyn* 49:2695–2704. <https://doi.org/10.1007/s00382-016-3475-y>
- Kay JE, Deser C, Phillips A, Mai A, Hannay C, Strand G, Arblaster JM, Bates SC, Danabasoglu G, Edwards J, Holland M, Kushner P, Lamarque J-F, Lawrence D, Lindsay K, Middleton A, Munoz E, Neale R, Oleson K, Polvani L, Vertenstein M (2015) The community earth system model (CESM) large ensemble project: a community resource for studying climate change in the presence of internal climate variability. *Bull Am Meteor Soc* 96:1333–1349. <https://doi.org/10.1175/BAMS-D-13-00255.1>
- Kug J-S, Choi J, An S-I, Jin F-F, Wittenberg AT (2010) Warm pool and cold tongue El Niño events as simulated by the GFDL 2.1 coupled GCM. *J Clim* 23:1226–1239. <https://doi.org/10.1175/2009JCLI3293.1>
- Lee T, McPhaden MJ (2010) Increasing intensity of El Niño in the central-equatorial Pacific. *Geophys Res Lett*. <https://doi.org/10.1029/2010GL044007>
- Lengaigne M, Hausmann U, Madec G, Menkes C, Vialard J, Molines JM (2012) Mechanisms controlling warm water volume interannual variations in the equatorial Pacific: diabatic versus adiabatic processes. *Clim Dyn* 38:1031–1046. <https://doi.org/10.1007/s00382-011-1051-z>
- Li G, Xie S-P (2013) Tropical biases in CMIP5 multimodel ensemble: the excessive equatorial pacific cold tongue and double ITCZ problems. *J Clim* 27:1765–1780. <https://doi.org/10.1175/JCLI-D-13-00337.1>
- Li G, Xie S-P, Du Y, Luo Y (2016) Effects of excessive equatorial cold tongue bias on the projections of tropical Pacific climate change. Part I: the warming pattern in CMIP5 multi-model ensemble. *Clim Dyn* 47:3817–3831. <https://doi.org/10.1007/s00382-016-3043-5>
- Liguori G, Di Lorenzo E (2018) Meridional modes and increasing pacific decadal variability under anthropogenic forcing. *Geophys Res Lett* 45:983–991. <https://doi.org/10.1002/2017GL076548>
- Maloney ED, Adames AF, Bui HX (2019) Madden-Julian oscillation changes under anthropogenic warming. *Nature Clim Change* 9(1):26–33. <https://doi.org/10.1038/s41558-018-0331-6>
- Matveeva T, Gushchina D, Dewitte B (2018) The seasonal relationship between intraseasonal tropical variability and ENSO in CMIP5. *Geosci Model Dev* 11:2373–2392. <https://doi.org/10.5194/gmd-11-2373-2018>
- McGregor S, Timmermann A, Jin F-F, Kessler WS (2016) Charging El Niño events with off-equatorial wind bursts. *Clim Dyn* 47:1111. <https://doi.org/10.1007/s00382-015-2891-8>
- McPhaden MJ, Zebiak SE, Glantz MH (2006) ENSO as an integrating concept in earth science. *Science* 314:1740–1745. <https://doi.org/10.1126/science.1132588>
- McPhaden MJ, Lee T, McClurg D (2011) El Niño and its relationship to changing background conditions in the tropical Pacific Ocean. *Geophys Res Lett*. <https://doi.org/10.1029/2011GL048275>
- Meehl GA, Boer GJ, Covey C, Latif M, Stouffer RJ (2000) The coupled model intercomparison project (CMIP). *Bull Am Meteor Soc* 81:313–318
- Meehl GA, Washington WM, Arblaster JM, Hu A, Teng H, Kay JE, Gettelman A, Lawrence DM, Sanderson BM, Strand WG (2013) Climate change projections in CESM1(CAM5) compared to CCSM4. *J Clim* 26:6287–6308. <https://doi.org/10.1175/JCLI-D-12-00572.1>
- Neske S, McGregor S (2018) Understanding the warm water volume precursor of ENSO events and its interdecadal variation. *Geophys Res Lett*. <https://doi.org/10.1002/2017GL076439>
- Oleson W, Lawrence M, Bonan B, Flanner G, Kluzek E, Lawrence J, Levis S, Swenson C, Thornton E, Dai A, Decker M, Dickinson R, Feddesma J, Heald L, Hoffman F, Lamarque J-F, Mahowald N, Niu G-Y, Qian T, Randerson J, Running S, Sakaguchi K, Slater A, Stockli R, Wang A, Yang Z-L, Zeng X, Zeng X (2010) Technical description of version 4.0 of the community land model (CLM). <https://doi.org/10.5065/d6fb50wz>
- Philander SGH (1978) Forced oceanic waves. *Rev Geophys* 16:15–46. <https://doi.org/10.1029/RG016i001p00015>
- Power S, Delage F, Chung C, Kociuba G, Keay K (2013) Robust twenty-first-century projections of El Niño and related precipitation variability. *Nature* 502:541–545. <https://doi.org/10.1038/nature12580>
- Rayner NA (2003) Global analyses of sea surface temperature, sea ice, and night marine air temperature since the late nineteenth century. *J Geophys Res* 108:4407. <https://doi.org/10.1029/2002JD002670>
- Ren H-L, Jin F-F (2011) Niño indices for two types of ENSO. *Geophys Res Lett*. <https://doi.org/10.1029/2010GL046031>
- Richter I (2015) Climate model biases in the eastern tropical oceans: causes, impacts and ways forward. *Wiley Interdiscipl Rev Clim Change* 6:345–358. <https://doi.org/10.1002/wcc.338>
- Ropelewski CF, Halpert MS (1987) Global and regional scale precipitation patterns associated with the El Niño/Southern oscillation. *Mon Weather Rev* 115:1606–1626. [https://doi.org/10.1175/1520-0493\(1987\)115%3c1606:GARSPP%3e2.0.CO;2](https://doi.org/10.1175/1520-0493(1987)115%3c1606:GARSPP%3e2.0.CO;2)
- Santoso A, McGregor S, Jin F-F, Cai W, England MH, An S-I, McPhaden MJ, Guilyardi E (2013) Late-twentieth-century

- emergence of the El Niño propagation asymmetry and future projections. *Nature* 504:126–130. <https://doi.org/10.1038/nature12683>
- Smith R, Jones P, Briegleb B, Bryan F, Danabasoglu G, Dennis J, Dukowicz J, Eden C, Fox-Kemper B, Gent P et al (2010) The parallel ocean program (POP) reference manual ocean component of the community climate system model (CCSM) and community earth system model (CESM). In: Los Alamos National Laboratory Tech. Rep. LAUR-10-01853, vol 141, pp 1–140
- Stein K, Schneider N, Timmermann A, Jin F-F (2010) Seasonal synchronization of ENSO events in a linear stochastic model. *J Clim* 23:5629–5643. <https://doi.org/10.1175/2010JCLI3292.1>
- Stevenson S, Capotondi A, Fasullo J, Otto-Bliesner B (2017) Forced changes to twentieth century ENSO diversity in a last Millennium context. *Clim Dyn*. <https://doi.org/10.1007/s00382-017-3573-5>
- Takahashi K, Dewitte B (2016) Strong and moderate nonlinear El Niño regimes. *Clim Dyn* 46:1627–1645. <https://doi.org/10.1007/s00382-015-2665-3>
- Takahashi K, Montecinos A, Goubanova K, Dewitte B (2011) ENSO regimes: reinterpreting the canonical and Modoki El Niño. *Geophys Res Lett*. <https://doi.org/10.1029/2011GL047364>
- Takahashi K, Karamperidou C, Dewitte B (2018) A theoretical model of strong and moderate El Niño regimes. *Clim Dyn*. <https://doi.org/10.1007/s00382-018-4100-z>
- Taylor KE, Stouffer RJ, Meehl GA (2012) An overview of CMIP5 and the experiment design. *Bull Am Meteor Soc* 93:485–498. <https://doi.org/10.1175/BAMS-D-11-00094.1>
- Thuat S, Dewitte B, An S-I, Ayoub N (2011) Sensitivity of ENSO to stratification in a recharge-discharge conceptual model. *J Clim* 24:4332–4349. <https://doi.org/10.1175/2011JCLI4148.1>
- Thuat S, Dewitte B, An S-I, Illig S, Ayoub N (2013) Influence of recent stratification changes on ENSO stability in a conceptual model of the equatorial pacific. *J Clim* 26:4790–4802. <https://doi.org/10.1175/JCLI-D-12-00363.1>
- Trenberth KE, Stepaniak DP (2001) Indices of el Niño evolution. *J Clim* 14:1697–1701
- Vecchi GA, Harrison DE (2006) The Termination of the 1997–98 El Niño. Part I: mechanisms of oceanic change. *J Clim* 19:2633–2646. <https://doi.org/10.1175/JCLI3776.1>
- Vecchi GA, Soden BJ (2007) Global warming and the weakening of the tropical circulation. *J Clim* 20:4316–4340. <https://doi.org/10.1175/JCLI4258.1>
- Wittenberg AT, Rosati A, Lau N-C, Ploshay JJ (2006) GFDL's CM2 global coupled climate models. Part III: tropical pacific climate and ENSO. *J Clim* 19:698–722. <https://doi.org/10.1175/JCLI3631.1>
- Xie S-P, Peng Q, Kamae Y, Zheng X-T, Tokinaga H, Wang D (2018) Eastern pacific ITCZ dipole and ENSO diversity. *J Clim* 31:4449–4462. <https://doi.org/10.1175/JCLI-D-17-0905.1>
- Yeh S-W, Kug J-S, Dewitte B, Kwon M-H, Kirtman BP, Jin F-F (2009a) El Niño in a changing climate. *Nature* 461:511–514. <https://doi.org/10.1038/nature08316>
- Yeh S-W, Yim BY, Noh Y, Dewitte B (2009b) Changes in mixed layer depth under climate change projections in two CGCMs. *Clim Dyn* 33:199–213. <https://doi.org/10.1007/s00382-009-0530-y>
- Yeh S-W, Dewitte B, Yim BY, Noh Y (2010) Role of the upper ocean structure in the response of ENSO-like SST variability to global warming. *Clim Dyn* 35:355–369. <https://doi.org/10.1007/s00382-010-0849-4>
- Yeh S-W, Cai W, Min S-K, McPhaden MJ, Dommenges D, Dewitte B, Collins M, Ashok K, An S-I, Yim B-Y, Kug J-S (2018) ENSO atmospheric teleconnections and their response to greenhouse gas forcing. *Rev Geophys* 56:185–206. <https://doi.org/10.1002/2017RG000568>
- Zebiak SE, Cane MA (1987) A model El Niño-southern oscillation. *Mon Weather Rev* 115:2262–2278. [https://doi.org/10.1175/1520-0493\(1987\)115%3c2262:AMENO%3e2.0.CO;2](https://doi.org/10.1175/1520-0493(1987)115%3c2262:AMENO%3e2.0.CO;2)
- Zelle H, Appeldoorn G, Burgers G, van Oldenborgh GJ (2004) The Relationship between sea surface temperature and thermocline depth in the eastern equatorial pacific. *J Phys Oceanogr* 34:643–655. <https://doi.org/10.1175/2523.1>
- Zheng Y, Lin J-L, Shinoda T (2012) The equatorial Pacific cold tongue simulated by IPCC AR4 coupled GCMs: upper ocean heat budget and feedback analysis. *J Geophys Res* 117:C05024. <https://doi.org/10.1029/2011JC007746>
- Zheng X-T, Hui C, Yeh S-W (2018) Response of ENSO amplitude to global warming in CESM large ensemble: uncertainty due to internal variability. *Clim Dyn* 50:4019. <https://doi.org/10.1007/s00382-017-3859-7>

**Publisher's Note** Springer Nature remains neutral with regard to jurisdictional claims in published maps and institutional affiliations.

## Affiliations

Aude Carréric<sup>1,2</sup>  · Boris Dewitte<sup>1,3,4,5</sup> · Wenju Cai<sup>6,7</sup> · Antonietta Capotondi<sup>8,9</sup> · Ken Takahashi<sup>10</sup> · Sang-Wook Yeh<sup>11</sup> · Guojian Wang<sup>6,7</sup> · Virginie Guémas<sup>12</sup>

<sup>1</sup> LEGOS, Université de Toulouse, CNES, CNRS, IRD, UPS, Toulouse, France

<sup>2</sup> Barcelona Supercomputing Center (BSC), Barcelona, Spain

<sup>3</sup> Centro de Estudios Avanzados en Zonas Áridas (CEAZA), La Serena, Chile

<sup>4</sup> Facultad de Ciencias del Mar, Universidad Católica del Norte, Coquimbo, Chile

<sup>5</sup> Millennium Nucleus Ecology and Sustainable Management of Oceanic Island (ESMOI), Coquimbo, Chile

<sup>6</sup> Key Laboratory of Physical Oceanography, Institute for Advanced Ocean Studies, Ocean University of China and Qingdao National Laboratory for Marine Science and Technology, Qingdao, China

<sup>7</sup> Centre for Southern Hemisphere Oceans Research (CSHOR), CSIRO Oceans and Atmosphere, Hobart, TAS, Australia

<sup>8</sup> Cooperative Institute for Research in Environmental Science, University of Colorado, Boulder, CO, USA

<sup>9</sup> Physical Sciences Division, NOAA Earth System Research Laboratory, Boulder, CO, USA

<sup>10</sup> Servicio Nacional de Meteorología e Hidrología del Perú—SENAMHI, Lima, Peru

<sup>11</sup> Department of Marine Sciences and Convergent Technology, Hanyang University, Ansan, South Korea

<sup>12</sup> CNRM UMR 3589, Météo-France, CNRS, Toulouse, France